

1
2
3
4
5
6
7
8
9
10
11
12
13
14
15
16
17
18
19
20
21
22
23
24
25

**Contributions to OH reactivity from unexplored volatile organic compounds measured by
PTR-ToF-MS– A case study in a suburban forest of the Seoul Metropolitan Area during
KORUS-AQ 2016**

Dianne Sanchez,¹ Roger Seco,^{1*} Dasa Gu,¹ Alex Guenther,¹ John Mak,² Youngjae Lee,³ Danbi
Kim,³ Joonyoung Ahn,³ Don Blake,⁴ Scott Herndon,⁵ Daun Jeong,¹ John T. Sullivan,⁶ Thomas
Mcgee,⁶ and Saewung Kim^{1*}

1. Department of Earth System Science, University of California, Irvine, Irvine CA 92697,
U.S.A.

2. School of Marine and Atmospheric Sciences, Stony Brooke University, Stony Brook, NY
11794, U.S.A.

3. National Institute of Environmental Research, Inchoen 22689, South Korea

4. Department of Chemistry, University of California, Irvine, Irvine CA 92697, U.S.A.

5. Aerodyne Research Inc., Billerica MA 01821, U.S.A.

6. NASA Goddard Space Flight Center, Chemistry and Dynamics Laboratory, Greenbelt, MD
20771, U.S.A.

* Now at: Terrestrial Ecology Section, Department of Biology, University of Copenhagen,
Copenhagen, Denmark and
Center for Permafrost (CENPERM), Department of Geosciences and Natural Resource
Management, University of Copenhagen, Copenhagen, Denmark

Corresponding author: saewung.kim@uci.edu, tel 1-949-824-4531

To be submitted to Atmospheric Chemistry and Physics

26 **Abstract**

27

28 We report OH reactivity observations by a chemical ionization mass spectrometer –
29 comparative reactivity method (CIMS-CRM) instrument in a suburban forest of the Seoul
30 Metropolitan Area (SMA) during Korea US Air Quality Study (KORUS-AQ 2016) from mid-
31 May to mid-June of 2016. A comprehensive observational suite was deployed to quantify
32 reactive trace gases inside of the forest canopy including a high-resolution proton transfer
33 reaction time of flight mass spectrometer (PTR-ToF-MS). An average OH reactivity of $30.7 \pm$
34 5.1 s^{-1} was observed, while the OH reactivity calculated from CO, NO + NO₂ (NO_x), ozone (O₃),
35 sulfur dioxide (SO₂), and 14 volatile organic compounds (VOCs) was $11.8 \pm 1.0 \text{ s}^{-1}$. An analysis
36 of 346 peaks from the PTR-ToF-MS accounted for an additional $6.0 \pm 2.2 \text{ s}^{-1}$ of the total
37 measured OH reactivity, leaving 42.0 % missing OH reactivity. A series of analyses indicates
38 that the missing OH reactivity most likely comes from VOC oxidation products of both biogenic
39 and anthropogenic origin.

40

41

42

43

44

45

46

47

48

49

50 **1. Introduction**

51 Total OH reactivity (s^{-1}), the inverse of OH lifetime, is a measure of the total amount of
52 reactive trace gases in the atmosphere in the scale of reactivity, which allow us to quantitatively
53 evaluate our ability to constrain trace gases by comparing measurements of total OH reactivity
54 with the OH reactivity calculated from a speciated reactive gas measurement dataset. The
55 fraction of observed OH reactivity that cannot be reconciled by calculated OH reactivity is
56 known as “missing OH reactivity” (Di Carlo et al., 2004; Goldstein and Galbally, 2007; Yang et
57 al., 2016). A substantial amount of missing OH reactivity has consistently been reported in
58 forest environments (30 - 80%). Di Carlo et al. (2004) conducted a study in a mixed forest near
59 Pellston, Michigan where they reported missing OH reactivity (~ 30 %) larger than observational
60 uncertainty. The authors concluded that the missing sources of reactivity were primary biogenic
61 volatile organic compound (biogenic VOC, BVOC) emissions, as the degree of missing OH
62 reactivity followed the temperature dependence of terpenoid emissions. In a boreal forest in
63 Hyytiälä, Finland, Sinha et al. (2010) report a similar result with observed trace gases that
64 account for only 50% of the measured OH reactivity. They argued that oxidation products of
65 BVOCs alone could not account for the missing OH reactivity. Thus, they also concluded that
66 primary emissions were more likely to be the source of missing OH reactivity and they further
67 suggest that this could be the result of the contribution of small amounts of many reactive gases.
68 Follow up studies (Nolscher et al., 2012; Praplan et al., 2019) at the same site have presented a
69 consistent conclusion. Nolscher et al. (2012) observed the highest level of missing OH reactivity
70 during a heat wave episode, possibly inducing a stress emission response from the local forest. A
71 comprehensive analysis by Praplan et al. (2019) using a long-term observation dataset and a

72 photochemical model framework with the Master Chemical Mechanism illustrates that the model
73 simulated oxidation compound contribution can only contribute 7 % of missing OH reactivity.

74 On the other hand, some studies have attributed the sources of the missing OH reactivity
75 to unmeasured oxidation products of well-characterized BVOCs. Edwards et al. (2013)
76 measured OH reactivity in a pristine tropical forest in the Sabah region of Borneo during the
77 Oxidant and Particle Photochemical Processes (OP3) field campaign (Hewitt et al., 2010). This
78 study implemented the Master Chemical Mechanism (MCMv3.2) (Saunders et al., 2003; Jenkin
79 et al., 1997) into a box model framework to quantify potential contributions from unmeasured
80 oxidation products. The model was constrained with VOCs such as isoprene, monoterpenes, and
81 alkanes and alkenes and other observed trace gases such as $\text{NO} + \text{NO}_2$ (NO_x) and ozone (O_3).
82 The authors reported that the model simulated oxygenated VOCs (OVOCs) could contribute
83 47.1% of the calculated OH reactivity – surpassing the contribution from isoprene, the primary
84 emission of this ecosystem. It is notable that 30% of observed OH reactivity could not be
85 accounted for by the box model simulations. After examining the comprehensive observational
86 suite of VOCs, the authors determined that the most significant missing sources of OH reactivity
87 were likely secondary multifunctional carbon compounds rather than primary BVOC emissions.
88 Hansen et al. (2014) suggested that their observed missing OH reactivity were likely from
89 unmeasured oxidation products during the Community Atmosphere-Biosphere INteraction
90 EXperiment (CABINEX 2009) in Michigan. This notion was also consistent with findings
91 reported by Kim et al. (2011) who measured OH reactivity of branch enclosures from four
92 representative tree species in the forest canopy during the CABINEX study. They reconciled
93 most of the measured OH reactivity of four representative tree species with well-known BVOCs,
94 such as isoprene and monoterpenes. Finally, Nakashima et al. (2014) reported that 29.5% OH

95 reactivity could not be reconciled by the speciated trace gas dataset during the Bio-hydro-
96 atmosphere interactions of Energy, Aerosols, Carbon, H₂O, Organics and Nitrogen-Southern
97 Rocky Mountain 2008 (BEACHON-SMR08) field campaign (Ortega et al., 2014). The campaign
98 took place at the Manitou Experimental Forest (MEF) in Colorado, a ponderosa pine plantation
99 dominated by primary BVOC emissions of 2-methyl-3-butene-2-ol (232-MBO) and
100 monoterpenes (Ortega et al., 2014). The authors also reported that the missing OH reactivity was
101 likely from BVOC oxidation products. In the same context, Kim et al. (2010) conducted PTR-
102 MS mass spectrum analysis for both ambient air and branch enclosures at the MEF site. They
103 reported more conspicuous unidentified signals on PTR-MS mass spectra in the ambient samples
104 than those from branch enclosure samples at this site.

105 During the Southern Oxidant and Aerosol Study (SOAS) in 2013, Kaiser et al. (2016)
106 used a comprehensive suite of VOC measurements at an isoprene dominant forest site in the
107 southeastern US to examine the role of the OVOC species in missing reactive carbon. The
108 authors used MCMv3.2 embedded in the University of Washington Chemical Box Model
109 (UWCM) to compare OH reactivity from model-generated OVOCs to OH reactivity from
110 measurements of OVOCs. There was no significant discrepancy between the average measured
111 and calculated OH reactivity including observed trace gases and model calculated oxidation
112 products of VOCs. However, it was noted that a small portion (1 s^{-1}) of observed OH reactivity
113 could not be reconciled by the model calculation. As this fraction was not correlated to isoprene
114 oxidation products, it was suggested that the missing OH reactivity may be due to unmeasured
115 primary emissions. One caveat of this analysis pointed out by the authors was that the
116 concentrations of the modeled first-generation isoprene oxidation products (e.g. MVK, MACR,
117 isoprene hydroxy hydroperoxides (ISOPOOH), isoprene nitrates (ISOPN), and hydroperoxy

118 aldehydes (HPALD)) were significantly overpredicted in the afternoon. Consequently, the
119 uncertainty of the model calculation is likely to be much higher for the multi-generation
120 oxidation products and their contributions to the OH reactivity contributions. This result
121 highlights the uncertainty in relying solely on box-model results to assess OH reactivity. This
122 *status quo* urges us to take a convergent approach by effectively integrating observational results
123 from novel instrumentation and model outcomes.

124 This study examines the OH reactivity observations at Taehwa Research Forest (TRF)
125 supersite from 15 May 2016 to 7 June 2016 during the Korea United States Air Quality Study
126 2016 (KORUS-AQ 2016) campaign. TRF (37° 18' 19.08" N 127° 19' 7.12" E, 162 m altitude) is
127 operated by Seoul National University and located in Gwangju in the Gyunggi Province in South
128 Korea (Kim et al., 2013b). The site is about 35 km southeast from the center of Seoul and
129 borders the greater Seoul Metropolitan Area (SMA) with its population of 25.6 million. This
130 geographical proximity to SMA results in a significant level of anthropogenic influence,
131 particularly in elevated NO_x (Kim et al., 2016). Additionally, occasional pollution transport
132 events occur at regional scales. Previous studies at the site have consistently highlighted the
133 importance of BVOC photochemistry at TRF (Kim et al., 2016; Kim et al., 2013a; Kim et al.,
134 2015). Isoprene and monoterpenes are the dominant OH sinks at the site among observed VOCs.
135 The elevated NO_x accelerates the photochemical processing of VOCs (Kim et al., 2015). Thus,
136 this site is an ideal natural laboratory to study contributions towards total OH reactivity from
137 primary trace gas emissions from both natural and anthropogenic processes and their oxidation
138 products. This motivated us to deploy a high-resolution proton transfer reaction time-of-flight
139 mass spectrometer (PTR-ToF-MS) to quantify trace amounts of VOCs with unknown molecular
140 structures by taking advantage of the universal sensitivity of hydronium ion chemistry towards

141 reactive VOCs (Graus et al., 2010; Jordan et al., 2009a). Therefore, we intend to observationally
142 constrain the contributions of conventionally unidentified or unmeasured VOCs towards OH
143 reactivity.

144

145 **2. Methods**

146 **2.1. Field Site**

147 The Taehwa Research Forest is a Korean pine (*Pinus koraiensis*) plantation (300 m × 300
148 m) surrounded by a deciduous forest dominated by oak trees (Kim et al., 2013b). A flux tower
149 (40 m height) at the center of TRF has air-sampling inlets at multiple heights (4 m, 8 m 12 m,
150 and 16 m) below the canopy top (20 m). Each inlet consists of Teflon tubing (3/8" OD) with ~ 1
151 second of residence time. The trace gas dataset including VOCs presented is the average of
152 concentrations measured at the inlets inside of the canopy as previous studies illustrate that there
153 is no substantial vertical VOC gradients inside of the canopy (within 3 %, Kim et al. (2013b)).
154 An air-conditioned instrument shack located at the base of the flux tower housed the PTR-ToF-
155 MS for VOC measurements, a mini tunable infrared laser direct absorption spectroscopy (mini-
156 TILDAS) instrument for HCHO, methane, and methanol measurements, and analyzers for
157 carbon monoxide (CO), sulfur dioxide (SO₂), ozone (O₃), and meteorological measurements. The
158 OH reactivity and NO_x analyzers were located in another nearby air-conditioned shack (3 m
159 apart) and sampled air through an extended Teflon inlet line of 4 m (1/4" OD) from the ground
160 with a flow rate of 4 sLpm resulting in a 0.5 second residence time. The height of the ambient air
161 intake was 3.5 m. The analytical characteristics of the instrumentation suite are summarized in
162 Table 1. A ceilometer backscattering characterized boundary layer vertical structure at the site.
163 The ceilometer analysis described by Sullivan et al. (2019) reveals the diurnal boundary layer

164 height evolution, indicating a maximum in the afternoon around 1-3 km and a minimum in the
165 early morning below 500 m.

166

167 **2.2. OH Reactivity Measurements**

168 A chemical ionization mass spectrometer – comparative reactivity method (CIMS-CRM)
169 instrument was used to measure OH reactivity. The UCI CIMS-CRM system includes a chemical
170 ionization mass spectrometer with a hydronium reagent ion. The CRM method measures total
171 OH reactivity by quantifying the relative loss of pyrrole, a highly reactive gas ($k_{\text{OH}^+ \text{pyrrole}} = 1.07$
172 $\times 10^{-10} \text{ cm}^3 \text{ molecule}^{-1} \text{ s}^{-1}$ at 298 K (Dillon et al., 2012)) that is rarely found in the atmosphere
173 (Sinha et al., 2008b). Nitrogen gas flows through a bubbler full of ultrapure liquid
174 chromatography mass spectrometer (LC-MS) grade water to produce water vapor. The water
175 vapor then flows into a glass reactor where it is photolyzed into OH radicals by a mercury lamp
176 (Pen-Ray® Light Source P/N 90-0012-01). The measurement uncertainty is 16.7% (1σ) with a
177 limit of detection of 4.5 s^{-1} over 2 minutes (3σ).

178 The UCI CIMS-CRM instrument has been deployed on multiple occasions, including the
179 Megacity Air Pollution Study (MAPS)-Seoul 2015 campaign that incorporated previous
180 measurements at the TRF ground site during September 2015 (Sanchez et al., 2018; Kim et al.,
181 2016). During the SOAS 2013 campaign, an ambient OH reactivity intercomparison study was
182 conducted with laser induced fluorescence (LIF) system (Sanchez et al., 2018). The instrument
183 intercomparison showed that the OH reactivity measurements from the CRM and LIF
184 instruments generally agreed within the analytical uncertainty. An average of 16% difference
185 between the techniques was noted in the late afternoons where the CRM measurements were
186 lower than those from LIF. As discussed in Sanchez et al. (2018), this is likely caused by the

187 difference in sampling strategies, as the CRM measurements relied on a lengthy Teflon inlet (15
188 m) while the LIF directly sampled air at the top of a walk up tower. As mentioned above, at TRF
189 we used a shorter inlet line to minimize residence time and avoid inlet line loss.

190 An extensive intercomparison study was conducted by Fuchs et al. (2017) with various
191 OH reactivity measurement techniques that highlighted potential analytical artifacts in the CRM
192 technique. These artifacts have all been examined and preventive measures have been
193 implemented in the UCI CIMS-CRM system deployed at TRF. This included a laboratory-built
194 catalytic converter (Pt-wool at 350 °C) that minimized the interferences due to changes in air to
195 prevent the interference from the difference in humidity for the zero air characterizations.
196 Hansen et al. (2015) illustrated that NO_x may be generated from the catalytic converter. To
197 prevent potential NO_x interferences, they used a scrubber with Purafil and activated charcoal,
198 which will modulate the humidity in the sample. Our approach to this type of interference has
199 been to determine the maximum NO level, noticeably interfering with the calibration regression
200 line shown in Sanchez et al. (2018). Laboratory tests indicate that the statistical agreement
201 started to veer off when the NO level is 5 ppb in 1 σ of the linear regression between instrument
202 response (unitless) and OH reactivity (s⁻¹) as the slope for the calibration curve has changed from
203 0.238 to 0.246. In addition, Kim et al. (2016) achieved an OH reactivity budget closure in high
204 NO₂ condition, which implies no significant interferences from NO₂. However, in response to the
205 Fuchs et al. (2017) observation that various CRM configurations suffer from different levels of
206 NO_x interferences, we plan to conduct more systematic NO_x interference tests to more
207 accurately characterize this system. In conclusion, it is possible that our reported OH reactivity
208 may systematically underestimate ambient total OH reactivity as much as ambient OH reactivity
209 coming from NO₂.

210 We consistently kept the pyrrole to OH ratio at 3:1 and so did not achieve a pseudo first
211 order relationship. Even in the field environment with various relative humidity, we have not
212 observed noticeable changes in this ratio as we flow bulk humidified nitrogen (150 standard cc
213 per minute) to the reactor with the total flow of 240 cc, which result in dampening the temporal
214 ambient relative humidity variations. Therefore, we performed multi-point calibrations (5 s^{-1} to
215 30 s^{-1}) with a propene mixture using a NIST traceable gas standard (AirLiquide LLC, 0.847
216 ppm) during the field campaign to avoid any circumstances where the pseudo first-order reaction
217 regime is not established. Detailed calibration procedures for the OH reactivity system including
218 laboratory multi-component calibration results can be found in Sanchez et al. (2018).

219 In addition, Fuchs et al. (2017) also described a potential interference from ambient O_3 in
220 some CRM systems. In the 2015 field campaigns conducted in Seoul South Korea (Kim et al.,
221 2016), we conducted a standard addition experiment for the propene standard for additional ~ 30
222 s^{-1} in two different ozone environment 65 ppb and 123 ppb. The outcome illustrates an
223 agreement between two additions within the analytical uncertainty although a systematic
224 laboratory study will warrant an accurate uncertainty assessment from ozone. Again, as the CRM
225 method is a relatively new technique, one should keep in mind that the future studies may find
226 potential artifacts that we do not report in this study.

227

228 ***2.3.PTR-ToF-MS Measurements***

229 A high-resolution PTR-TOF-MS (Ionicon Analytik GmbH) (de Gouw and Warneke,
230 2007b) (Jordan et al., 2009b) was deployed at the TRF site. The instrument was operated with a
231 drift tube temperature of $60\text{ }^\circ\text{C}$, 560 V drift voltage, and 2.27 mbar drift tube to maintain E/N of
232 126 Td. Background checks were manually conducted about three times a day for a 10-minute

233 duration by scrubbing the ambient air through a catalytic convertor (Pt-wool maintained at
 234 350°C). The detectable peaks from the ambient spectra were assessed by subtracting the
 235 background spectrum. The instrument was calibrated with a gas mixture manufactured by Apel-
 236 Riemer Environmental Inc. The mixture contains ~ 1 ppmv of acetaldehyde, acetone, isoprene,
 237 methyl vinyl ketone, methacrolein, benzene, methyl ethyl ketone, toluene, o-xylene, and α -
 238 pinene. This standard mixture was only used for the PTR-ToF-MS calibration and not the CRM-
 239 CIMS calibration. The concentration of the compounds were assessed in the Blake Lab at
 240 University of California, Irvine, who also conducted the airborne VOC analysis using whole air
 241 samples during the KORUS-AQ campaign on the NASA DC-8 (Colman et al., 2001).

242 A mass range of m/z 40 to m/z 267 was analyzed from the recorded PTR-ToF-MS mass
 243 spectra. An automatic mass scale calibration was conducted every 5 minutes on the data
 244 averaged over 30 seconds. The raw PTR-ToF-MS data were processed using the PTRwid
 245 software described by Holzinger (2015). We normalized the mass peaks by 10^6 reagent ion
 246 counts (H_3O^+). As the majority of the VOC mass peaks could not be directly calibrated, we
 247 determined the VOC sensitivities using equation 1 (Eq 1). This method has been employed by a
 248 number of previous studies such as Cappellin et al. (2012). The benzene calibration factor was
 249 used to calculate mixing ratios by applying its proton transfer reaction rate coefficient ($k_{benzene}$
 250 $cm^3 s^{-1}$) and sensitivity ($S_{benzene} ncps ppb^{-1}$) for the available compounds. The application of this
 251 equation can be justified since PTRwid provides the mass discrimination corrected counts as a
 252 final computational product.

$$ppb_{VOC} = ncps_{VOC} \times \frac{k_{benzene}}{k_{VOC}} \times \frac{1}{11.94 ncps ppb^{-1}} \quad \text{Eq. 1}$$

253 where, 11.94 ncps ppb-1 is the assessed sensitivity of benzene.

Formatted: Not Superscript/ Subscript

Deleted: ncps ppb⁻¹

Formatted: Superscript

Formatted: Superscript

Formatted: Subscript

Formatted: Not Superscript/ Subscript

Formatted: Superscript

257 ppb_{VOC} is the mixing ratio of an analyte.
258 $ncps_{VOC}$ is the mass discrimination corrected normalized count for an analyte.
259 $k_{benzene}$ is the proton transfer reaction rate constant for benzene.
260 k_{VOC} is the proton transfer reaction rate constant for an analyte.

261

262 For the mass peaks where specific proton transfer reaction rates were unavailable, we
263 estimated the mixing ratios by applying a proton transfer reaction rate coefficient ($k_{H_3O^+}$) of 3.00
264 $\times 10^{-9} \text{ cm}^3 \text{ s}^{-1}$, the default value for PTRwid calculations. The spectra had a limit of detection of
265 tens of ppt for a 30 second average. The calibrated compounds had a range of detection limits as
266 low as 3.7 ppt for α -pinene and as high as 48 ppt for toluene.

267

268 **2.4. OH Reactivity Calculation**

269 OH reactivity was calculated from the concentrations of all the compounds observed by
270 the instrumental suite described in Table 1. The original data can be found in the KORUS-AQ
271 2016 data archive at <https://korus-aq.larc.nasa.gov/>. A total of 360 mass peaks measured by the
272 PTR-ToF-MS were analyzed above the background (3σ or above) to assess their contribution to
273 the calculated OH reactivity. Fourteen of the mass peaks were identified as VOCs commonly
274 reported for PTR-MS measurements (Table 1), leaving 346 unidentified peaks. These remaining
275 mass peaks were grouped into three categories in order to estimate their possible OH reactivity
276 contribution.

277 Category I (81 peaks) included mass peaks for which the PTRwid software calculated a
278 molecular formula. OH reaction rate coefficients for the individual peaks were obtained from the
279 National Institute for Standards and Technology (NIST) Webbook library. As the only

280 information we have is the molecular composition, we identified multiple isomers with different
281 functional groups and thus different reactivity. We have extensively reviewed previous
282 publications (Williams et al., 2001;De Gouw et al., 2003;de Gouw and Warneke, 2007a;Jordan et
283 al., 2009a;Ruuskanen et al., 2011;Muller et al., 2012;Koss et al., 2017a) identifying ambient
284 VOCs using PTR-MS with both quadrupole and time-of-flight systems to identify possible
285 compounds. For example, for the m/z of 75.043, there are four possible compounds including
286 hydroxy acetone, propionic acid, methyl acetate, and ethyl formate. We used the median reaction
287 constant for the set of possible compounds. The detailed description of the OH reaction constant
288 determination process for the Category I peaks is described in Sanchez (2019). If the information
289 was unavailable from the NIST Webbook database, a structure-reactivity relationship described
290 by Kwok and Atkinson (1995) was applied to obtain reaction rate coefficients. This is an
291 empirical calculation system to estimate k_{OH} based upon the number of carbons and the
292 functional groups of given VOCs. The framework is able to calculate k_{OH} within a factor of two
293 according to a thorough assessments presented in Kwok and Atkinson (1995). However, the
294 authors discourage the application of the framework to compounds that were not examined in the
295 study such as halogenated compounds. Although halogenated compounds are not included in this
296 study, one should be aware of a potentially significant uncertainty.

297 Category II (28 peaks) included mass peaks for which the PTRwid software could not
298 assess an exact molecular composition due to uncertainty in the data processing system.
299 Nonetheless, this group of compounds illustrated a positive correlation ($R^2 = 0.19$ to 0.88) with
300 either anthropogenic (benzene, toluene) or biogenic (MVK+MACR and monoterpenes) VOCs.
301 Category II compounds are further grouped into subcategories corresponding to these two main
302 VOC sources. OH reaction rate constants (k_{OH}) were estimated with equations based on the

303 relationship between the m/z and the k_{OH} of compounds in Table 1 (Figure S1). More
304 specifically, we assume that k_{OH} is linearly correlated with m/z . To apply this linear relationship,
305 the compounds with known k_{OH} were grouped into 5 m/z bins and the average k_{OH} of each bin
306 was calculated. The green triangles represent 5 m/z binned averages from these compounds
307 plotted with their respective average k_{OH} . This approach can be justified by the fact that the
308 reaction constants of VOCs towards OH tend to increase as a function of molecular mass within
309 functional groups (Kwok and Atkinson, 1995; Atkinson, 1987). The y-intercepts of the linear
310 regressions were assessed using the k_{OH} values of the biogenic or anthropogenic compounds and
311 their masses.

312 Category III (237 peaks) included mass peaks with very low mixing ratios (average = 4.8
313 ppt \pm 19.5 ppt) that were above the limit of detection. We applied a k_{OH} corresponding to the dark
314 green best-fit line in Figure S1 to these peaks. The y-intercept of the dark green line was based
315 on that of acetaldehyde, as it was the lowest mass compound used for the OH reactivity
316 calculations in this study.

317 There are two components that need to be considered for the assessment of uncertainty
318 associated with calculated OH reactivity: the concentration and the reaction constants with OH.
319 The uncertainty of the observed trace gases is in the range of 5 % to 20 % as shown in Table 1
320 and is associated with the rate constants from laboratory experiments (Atkinson et al., 2006).
321 Combining 15 % uncertainty from reaction constants and 13.5 % from trace gas observations
322 results in 20 % of uncertainty in calculated OH reactivity. This should be considered as a
323 conservative estimate as most VOC concentrations and associated rate constants are empirically
324 estimated.

325

326 **3. Results and Discussion**

327 An average OH reactivity of $30.7 \pm 5.1 \text{ s}^{-1}$ was observed from 15 May – 7 June 2016
328 (Figure 1). This was within the range of OH reactivity observed in urban regions ($10 - 33 \text{ s}^{-1}$).
329 (Kovacs et al., 2003;Ren et al., 2003;Sinha et al., 2008a;Dolgorouky et al., 2012;Whalley et al.,
330 2016;Kim et al., 2016;Yang et al., 2017) and in the range of previously reported observations
331 and model calculations at the TRF site ($\sim 15 - 35 \text{ s}^{-1}$) (Kim et al., 2016;Kim et al., 2015). The
332 total calculated OH reactivity of $11.8 \pm 1.0 \text{ s}^{-1}$ from the measured compounds in Table 1 resulted
333 in 63.3% missing OH reactivity. However, an additional OH reactivity of $6.0 \pm 2.2 \text{ s}^{-1}$ was
334 further calculated from the reactivity of the VOCs in Categories I – III. The contribution lowered
335 the missing OH reactivity level to 42% of the measured OH reactivity. Kim et al. (2016) had
336 previously measured an average OH reactivity of 16.5 s^{-1} at TRF during the MAPS-Seoul
337 campaign from 1 September – 15 September 2015, a substantially lower level than what we
338 report during this springtime study. Although small alkanes and alkenes such as ethane, ethene,
339 propane and propene were not observed on the site, we utilized the dataset from the NASA DC-8
340 that flew at 700 m above the site, which indicates that their contribution was consistently small
341 ($\sim 0.7 \text{ s}^{-1}$ in average). In this suburban forest, we do not think there is any substantial emission
342 sources of these relatively long-lived VOCs.

343 The difference can be attributed to the notably higher reactive trace gas loadings during
344 KORUS-AQ compared to the TRF measurements during MAPS-Seoul. The NO_x , benzene, and
345 toluene concentrations were 3 times higher during KORUS-AQ and CO was 1.4 times higher
346 (Figure S2). Although the average isoprene concentrations were similar between the two
347 campaigns, MVK and MACR concentrations during KORUS-AQ were ~ 3 times higher,
348 illustrating a higher oxidative environment. There was a persistently high MVK+MACR to

349 isoprene ratio of 1.8 during the KORUS-AQ campaign at TRF. This ratio was similar to the
350 value reported during the summer in a moderately polluted forest in the Pearl River Delta that
351 was attributed to a strong atmospheric oxidation capacity (Gong et al., 2018). The missing OH
352 reactivity during KORUS-AQ was generally much higher than levels reported during urban
353 observations (up to 50% missing OH reactivity) (Kovacs et al., 2003;Ren et al., 2003;Sinha et
354 al., 2008a;Dolgorouky et al., 2012;Whalley et al., 2016;Kim et al., 2016;Yang et al., 2017) and
355 within the range of previously reported values in forest regions where as much as 80% missing
356 OH reactivity has been reported (Kim et al., 2016;Di Carlo et al., 2004;Nolscher et al.,
357 2012;Edwards et al., 2013;Nolscher et al., 2016;Ramasamy et al., 2018;Nakashima et al., 2014).

358 Figure 2 shows the diurnal average of measured, calculated, and missing OH reactivity
359 from 15 May – 7 June 2016. Isoprene was the largest contributor to VOC OH reactivity in the
360 afternoon and the early evening (36% of the calculated OH reactivity in the evening), consistent
361 with the previous studies conducted in this site (Kim et al., 2016;Kim et al., 2013b;Kim et al.,
362 2015). Among all the trace gases, the largest average contributor to the calculated OH reactivity
363 was NO_x, which contributed 18.2% (5.6 s⁻¹) to the measured OH reactivity. The NO_x
364 contribution to OH reactivity is higher during the morning and evening rush hours and at a
365 minimum in the afternoon, which has been reported consistently in previous reports conducted
366 near megacities (Kovacs et al., 2003;Mao et al., 2010;Dolgorouky et al., 2012;Ren et al.,
367 2003;Shirley et al., 2006). Enhanced OH reactivity during the morning or night and minimum
368 OH reactivity during the afternoon have been reported in urban areas (Kovacs et al., 2003;Ren et
369 al., 2006;Shirley et al., 2006;Dolgorouky et al., 2012;Mao et al., 2010;Whalley et al., 2016). On
370 the other hand, strong light-sensitive biogenic emissions (e.g. isoprene) result in a maximum
371 observed OH reactivity in the afternoon in forested regions (Ren et al., 2006;Sinha et al.,

372 2012;Edwards et al., 2013;Hansen et al., 2014;Zannoni et al., 2017;Nolscher et al., 2016) . One
373 exception is an OH reactivity observation conducted in Hyytiälä, a forested site that has low
374 isoprene levels, by Sinha et al. (2010). They attributed a flat diurnal OH reactivity variation to
375 the interplay between high daytime emissions and low nighttime boundary layer height. In urban
376 environments, it is mostly anthropogenic trace gases such as aromatics and OVOCs that
377 contribute to OH reactivity. These compounds have a longer lifetime compared to the diurnal
378 boundary layer evolution. This leads to the accumulation of such compounds in the shallow
379 boundary layer during the night. On the other hand, strong emissions of reactive BVOCs in
380 deciduous forest regions enhance OH reactivity during the daytime but then quickly react away.
381 Very subtle diurnal differences observed in this study (Figure 2), therefore, can be understood as
382 the competitive influences of both anthropogenic and biogenic compounds to the OH reactivity.

383 As described in detail in Sullivan et al. (2019) and Jeong et al. (2019), a strong regional
384 stagnation episode occurred during the KORUS-AQ campaign between May 17 – 23. Later, the
385 Korean Peninsula was affected by a period of continental pollution outflow between May 28 and
386 June 1. The diurnal averages of the two periods and their calculated OH reactivity are presented
387 in Figure 3. It is notable that there is very little difference in the observed OH reactivity between
388 the two distinct periods in terms of the amount of OH reactivity and its diurnal pattern (Figure 4).
389 Furthermore, no significant variance of the different classes of reactive gases such as criteria air
390 pollutants (CO, NO_x, O₃, and SO₂), mostly contributed by NO_x, OVOCs (acetone, acetaldehyde,
391 formaldehyde, methylglyoxal, methanol, methyl ethyl ketone), aromatics (benzene, toluene,
392 xylenes, styrene, benzaldehyde, trimethylbenzenes), and BVOCs (isoprene, monoterpenes,
393 sesquiterpenes, MVK+MACR) was observed during the different periods (Figure 5). These
394 different classes of reactive gases generally differed by less than 10% during the two periods

395 from the overall campaign. This observation shows that the presence of reactive gases is mostly
396 controlled by relatively short-lived compounds determined by local emissions and their oxidation
397 products.

398 The diurnal variation behavior of each chemical class reflects the chemical lifetime of the
399 compounds (e.g. aromatics vs BVOCs). The calculated OH reactivity from OVOCs does not
400 show a strong diurnal variation. This reflects the fact that OVOCs are mostly generated or
401 emitted during the daytime and their lifetime is generally longer than their precursors, which
402 allows nocturnal accumulation due to the absence of OH. The differences in the diurnal variation
403 of different classes of reactive gases can also be used to interpret the origin of the compounds in
404 Categories I-III as presented in Figure 6. The diurnal variations of Category I resemble those of
405 relatively long-lived chemical species with a distinct nocturnal accumulation pattern. This
406 diurnal pattern has been previously reported for both anthropogenic VOCs such as toluene and
407 benzene and temperature dependent monoterpenes such as α -pinene. It is notable that the diurnal
408 pattern is enhanced during the stagnation period during early morning hours. This enhancement
409 is also seen in the aromatic trace gases particularly during the stagnation period (Figure 5b).

410 Indeed, there are both biogenic and anthropogenic contributions towards the Category I
411 compounds, which contribute an average of 3.8 s^{-1} to the OH reactivity assessment, the largest
412 amount among the three categories (Figure 6a). The largest contributors to Category I, which
413 appear to be from a mixture of biogenic and anthropogenic sources, include m/z 89.060, 101.06,
414 and 101.096, and they contributed 0.3 s^{-1} , 0.2 s^{-1} , and 0.2 s^{-1} , respectively. The m/z 89.060 had a
415 molecular formula of $\text{C}_4\text{H}_8\text{O}_2\text{H}^+$ and was correlated to the anthropogenic compounds such as
416 benzene and toluene. The m/z 101.06 peak had the molecular formula of $\text{C}_5\text{H}_8\text{O}_2\text{H}^+$ and had a
417 diurnal variation similar to that of MVK + MACR. This mass peak has been previously

418 identified in laboratory (Zhao et al., 2004) and field (Williams et al., 2001) studies as the C₅
419 hydroxy carbonyl, an isoprene oxidation product. Results from an indoor chamber
420 photooxidation experiment conducted by Lee et al. (2006) showed that *m/z* 101 is a common
421 fragment of unidentified oxidation products of monoterpenes, sesquiterpenes, and isoprene. Lee
422 et al. (2006) also reported that this mass peak also composed over 5% of the fragments of
423 unidentified α - humulene and linalool oxidation products. The molecular formula of this peak is
424 C₆H₁₂OH⁺, and it has been identified in previous studies as C₆ carbonyls (Koss et al., 2017b) or
425 hexanal (Brilli et al., 2014; Rinne et al., 2005). Furthermore, *m/z* 99.044 and 113.023 were also
426 among the highest contributors to Category I and were correlated with MVK and MACR. The
427 *m/z* 99 was previously reported to be a fragment ion of unidentified terpene oxidation products in
428 a chamber experiment (Lee et al., 2006). The *m/z* 113 was observed by a PTR-MS in a
429 Ponderosa pine forest in central California by Holzinger et al. (2005). In this case, it was formed
430 within the canopy from the rapid oxidation of terpinolene, myrcene, and α -terpinene.
431 Furthermore, *m/z* 113 was observed to come from the photooxidation and ozonolysis of multiple
432 terpenes in two indoor chamber studies by Lee et al. (2006). The *m/z* 113 composed over 5% of
433 the oxidation product fragments of myrcene and verbenone. Finally, *m/z* 83.085 had the
434 molecular formula of C₆H₁₁⁺ and was correlated to benzene. Multiple studies have identified this
435 peak as cyclohexane, methyl-cyclopentane, or methylcyclohexane, typically found in areas rich
436 in oil and gas (Koss et al., 2017b; Gueneron et al., 2015; Yuan et al., 2014). In summary, both the
437 gross diurnal pattern and the individual peak analyses consistently illustrates that both
438 anthropogenic and biogenic compounds comprise Category I, the largest contributor to the
439 previously unexplored compounds in the PTR-ToF-MS spectrum at this research site.

440 Category II contributed an average of 0.3 s^{-1} to the calculated OH reactivity, the lowest
441 amount for the three Categories (Figure 6b). The compounds in category II appear to correlate to
442 either BVOCs or acetone, depending on the time period. In Figure 6b, the maximum during the
443 transport period is enhanced to about 0.2 s^{-1} higher than the overall campaign and shifted about 3
444 hours later to ~4:00 PM. The OH reactivity calculated from Category II is strongly correlated to
445 MVK + MACR ($r^2 = 0.82$) during this period as well. On the other hand, during the stagnation
446 period the average OH reactivity from Category II correlates more strongly with acetone ($r^2 =$
447 0.62) than with MVK +MACR ($r^2 = 0.28$). In fact, six of the highest contributors to Category II
448 (Figure 6b) are more strongly correlated to acetone ($r^2 > 0.40$) during the stagnation period
449 compared to the transport period. The sources of acetone can be either biogenic or
450 anthropogenic. Biogenic sources include direct emissions from plants or their oxidation products
451 and plant decay (Jacob et al., 2002;Seco et al., 2007). Anthropogenic sources of acetone include
452 vehicular emissions, solvent use, and the oxidation of other anthropogenic VOCs (Jacob et al.,
453 2002). Therefore, this illustrates that the compounds in Category II also have a complex source
454 profile of both biogenic and anthropogenic origin.

455 Category III contributed 1.9 s^{-1} to the calculated OH reactivity (Figure 6c). The six
456 highest contributors out of 236 mass peaks contributed a total of 0.43 s^{-1} of the calculated OH
457 reactivity. Overall, Category III compounds had no strong correlations to isoprene,
458 MVK+MACR, benzene, or toluene during either the stagnation or transport periods. However,
459 Category III compounds were highly correlated to methylglyoxal ($r^2 = 0.85, 0.82,$ and 0.78 for
460 the stagnation, transport, and overall period, respectively), one of the measured OVOCs. A
461 global modeling study illustrated that methylglyoxal is mainly produced from isoprene oxidation
462 processes and the second most important source is acetone oxidation (Fu et al., 2008). In

463 addition, aromatics and alkenes are also known to produce methylglyoxal through atmospheric
464 oxidation processes (Henry et al., 2012). As TRF is a high aromatics and high isoprene
465 environment, the source profile of methyl glyoxal in the region is likely complex, which can be
466 applied to interpret the source of the Category III compounds.

467 Overall, the OH reactivity estimates from Categories I – III contributed an average of 6.0
468 $\pm 2.2 \text{ s}^{-1}$ to the calculated OH reactivity. In summary, there is consistency that both
469 anthropogenic and the biogenic contributions need to be further studied in the PTR-ToF-MS
470 spectrum. Furthermore, by adding this additional signal from Category I, II, and III, VOC
471 contribution to calculated OH reactivity (11.0 s^{-1}) becomes larger than that (6.8 s^{-1}) from criteria
472 air pollutants (CO, NO_x, SO₂ and O₃). This should be considered when evaluating ozone
473 production regimes (Kim et al., 2018).

474 Even with the inclusion of the additional peaks to the calculated OH reactivity, we still
475 find a missing OH reactivity of 42%. Thus, it is important to investigate the origin of this
476 missing fraction. A correlation can be observed between missing OH reactivity in percentage and
477 OH reactivity from NO_x ($R^2 = 0.5$, Figure 7 A) but not between OH reactivity from NO_x and
478 absolute missing OH reactivity (s^{-1}) ($R^2 = 0.2$, Figure 7 B). This leads us to speculate that there
479 is a consistent presence of unquantified trace gases, likely oxidation products of both
480 anthropogenic and biogenic VOCs as we explored the origin of the unexplored peaks causing
481 missing OH reactivity. In other words, NO_x is relatively well measured with a highly pronounced
482 temporal variation that determines the percentage of missing OH reactivity.

483 Finally, unaccounted for uncertainty associated with the reaction rate constant
484 estimations described in the method section should be also further explored. For example, to
485 reconcile the averaged missing OH reactivity during the day (10 s^{-1}), it requires $\sim 60 \text{ ppm}$ of

486 methane but only ~ 4 ppb of isoprene. This clearly demonstrates the importance of rate constant
487 estimation. Indeed, if we apply the reaction rate constant of isoprene with OH ($k_{\text{OH}} = 1 \times 10^{-10}$
488 $\text{cm}^3 \text{ molecule}^{-1} \text{ s}^{-1}$ at 298 K) to Category II and Category III compounds, then the observed OH
489 reactivity is fully reconciled (Figure S3). Proton ion chemistry may have an intrinsic limitation to
490 quantify highly oxidized OVOCs. Moreover, due to the different inlet configurations for OH
491 reactivity and VOC observations, their contributions towards observed and calculated OH
492 reactivity may not have been consistently evaluated (e.g. Sanchez et al. (2018)). Therefore, a
493 comprehensive analysis along with a dataset from other instrumentation is necessary towards
494 reconciling missing OH reactivity with observational constraints. Finally, it is highly plausible
495 that we may double count for fragmented molecules in the mass spectrum. Although it would not
496 affect concentration evaluation as the intensity of ion signals from the fragmented molecules
497 would be fully accounted for by adding parent ion and fragmented ion signals, the OH reactivity
498 calculated from the fragmented ions is susceptible to underestimation from the assumption that
499 k_{OH} positively correlates with molecular masses.

500

501 **4. Summary**

502 We present OH reactivity observations at a suburban forest site during the KORUS-AQ field
503 campaign. A comprehensive trace gas dataset including 14 VOCs quantified by PTR-ToF-MS is
504 used to calculate OH reactivity, which only accounts for 36.7 % of the averaged observed OH
505 reactivity.

506 This study presents a detailed methodology for retrieving OH reactivity contributions from
507 all of the peaks of the PTR-ToF-MS mass spectrum. This decreases the amount of missing OH
508 reactivity as the majority of them have not been accounted towards calculated OH reactivity in

509 previous studies. First, we converted the raw signals to concentrations using a constant proton
510 transfer reaction rate ($3 \times 10^{-9} \text{ cm}^3 \text{ s}^{-1}$). Then, we grouped the previously unaccounted peaks into
511 three categories to estimate reaction constants for each compound. The contributions of the
512 unaccounted peaks in the mass spectrum account for a calculated OH reactivity of $\sim 6 \text{ s}^{-1}$, which
513 decreases missing OH reactivity from 63.3 % to 42.0 %. It is noteworthy that the diurnal
514 variations of observed OH reactivity and calculated OH reactivity from the various groups of
515 trace gases does not have a high variability during the field campaign even though there were
516 several synoptic meteorological configuration changes. This suggests that the reactive trace gas
517 loading is mostly determined by local emission and oxidation processes not influenced by the
518 synoptic meteorological conditions.

519 In conclusion, this study highlights PTR-ToF-MS as a tool for observationally constraining
520 missing OH reactivity. Further study is required particularly towards characterizing proton
521 reaction rate constants and reaction constants with OH for the many unknown compounds
522 detected on PTR-ToF-MS. In addition, other mass spectrometry techniques, such as nitrate or
523 iodine ion chemistry systems, should be utilized in future studies to complement the PTR
524 technique, which is sensitive to volatile to semi volatile VOCs, to quantify lower volatility
525 compounds and comprehensively constrain OH reactivity contributions from VOCs.

526

527 **Acknowledgements**

528

529 This study is supported by NASA (NNX15AT90G) and NIER. We highly appreciate NASA
530 ESPO for logistical support. Taehwa Research Forest is operated by College of Agriculture and
531 Life Sciences at Seoul National University. S. Kim would like to acknowledge a funding support

532 from Brain Pool Program of National Research Foundation Korea (NRF) Funded by the Ministry
533 of Science ICT (# 2020H1D3A2A01060699).

534

535 **Data Availability**

536

537 Data is available at: <https://korus-aq.larc.nasa.gov/>

538

539 **References**

540

- 541 Atkinson, R.: A Structure-Activity Relationship for the Estimation of Rate Constants for the
542 Gas-Phase Reactions of Oh Radicals with Organic-Compounds, *International Journal of*
543 *Chemical Kinetics*, 19, 799-828, DOI 10.1002/kin.550190903, 1987.
- 544 Atkinson, R., Baulch, D. L., Cox, R. A., Crowley, J. N., Hampson, R. F., Hynes, R. G., Jenkin,
545 M. E., Rossi, M. J., and Troe, J.: Evaluated kinetic and photochemical data for
546 atmospheric chemistry: Volume II - gas phase reactions of organic species, *Atmospheric*
547 *Chemistry and Physics*, 6, 3625-4055, 2006.
- 548 Brill, F., Gioli, B., Ciccioli, P., Zona, D., Loreto, F., Janssens, I. A., and Ceulemans, R.: Proton
549 Transfer Reaction Time-of-Flight Mass Spectrometric (PTR-TOF-MS) determination of
550 volatile organic compounds (VOCs) emitted from a biomass fire developed under stable
551 nocturnal conditions, *Atmospheric Environment*, 97, 54-67,
552 10.1016/j.atmosenv.2014.08.007, 2014.
- 553 Cappellin, L., Karl, T., Probst, M., Ismailova, K., Winkler, P. M., Soukoulis, C., Aprea, E.,
554 Mark, T. D., Gasperi, F., and Biasioli, F.: On quantitative determination of volatile
555 organic compound concentrations using proton transfer reaction Time-of-Flight Mass
556 Spectrometry, *Environment Science & Technology*, 46, 2012.
- 557 Colman, J. J., Swanson, A. L., Meinardi, S., Sive, B. C., Blake, D. R., and Rowland, F. S.:
558 Description of the analysis of a wide range of volatile organic compounds in whole air
559 samples collected during PEM-Tropics A and B, *Analytical Chemistry*, 73, 3723-3731,
560 2001.
- 561 De Gouw, J., Goldan, P., Warneke, C., Kuster, W., Roberts, J. M., Marchewka, M., Bertman, S.
562 B., Pszenny, A., and Keene, W.: Validation of proton transfer reaction-mass spectrometry
563 (PTR-MS) measurements of gas phase organic compounds in the atmosphere during the
564 New England Air Quality Study (NEAQS) in 2002, *Journal of Geophysical Research*,
565 108, 4682 doi:4610.1029/2003JD003863, 2003.
- 566 de Gouw, J., and Warneke, C.: Measurements of volatile organic compounds in the earths
567 atmosphere using proton-transfer-reaction mass spectrometry, *Mass Spectrom Rev*, 26,
568 223-257, 2007a.

569 de Gouw, J., and Warneke, C.: Measurements of volatile organic compounds in the earth's
570 atmosphere using proton-transfer-reaction mass spectrometry, *Mass Spectrom Rev*, 26,
571 223-257, 10.1002/mas.20119, 2007b.

572 Di Carlo, P., Brune, W. H., Martinez, M., Harder, H., Leshner, R., Ren, X. R., Thornberry, T.,
573 Carroll, M. A., Young, V., Shepson, P. B., Riemer, D., Apel, E., and Campbell, C.:
574 Missing OH reactivity in a forest: Evidence for unknown reactive biogenic VOCs,
575 *Science*, 304, 722-725, Doi 10.1126/Science.1094392, 2004.

576 Dillon, T. J., Tucceri, M. E., Dulitz, K., Horowitz, A., Vereecken, L., and Crowley, J. N.:
577 Reaction of Hydroxyl Radicals with C₄H₅N (Pyrrole): Temperature and Pressure
578 Dependent Rate Coefficients, *Journal of Physical Chemistry A*, 116, 6051-6058,
579 10.1021/jp211241x, 2012.

580 Dolgorouky, C., Gros, V., Sarda-Estève, R., Sinha, V., Williams, J., Marchand, N., Sauvage, S.,
581 Poulain, L., Sciare, J., and Bonsang, B.: Total OH reactivity measurements in Paris
582 during the 2010 MEGAPOLI winter campaign, *Atmospheric Chemistry and Physics*, 12,
583 9593-9612, Doi 10.5194/Acp-12-9593-2012, 2012.

584 Edwards, P. M., Evans, M. J., Furneaux, K. L., Hopkins, J., Ingham, T., Jones, C., Lee, J. D.,
585 Lewis, A. C., Moller, S. J., Stone, D., Whalley, L. K., and Heard, D. E.: OH reactivity in
586 a South East Asian tropical rainforest during the Oxidant and Particle Photochemical
587 Processes (OP3) project, *Atmospheric Chemistry and Physics*, 13, 9497-9514, Doi
588 10.5194/Acp-13-9497-2013, 2013.

589 Fu, T. M., Jacob, D. J., Wittrock, F., Burrows, J. P., Vrekoussis, M., and Henze, D. K.: Global
590 budgets of atmospheric glyoxal and methylglyoxal, and implications for formation of
591 secondary organic aerosols, *Journal of Geophysical Research-Atmospheres*, 113, 2008.

592 Fuchs, H., Novelli, A., Rolletter, M., Hofzumahaus, A., Pfannerstill, E. Y., Kessel, S., Edtbauer,
593 A., Williams, J., Michoud, V., Dusanter, S., Locoge, N., Zannoni, N., Gros, V., Truong,
594 F., Sarda-Estève, R., Cryer, D. R., Brumby, C. A., Whalley, L. K., Stone, D., Seakins, P.
595 W., Heard, D. E., Schoemaeker, C., Blocquet, M., Coudert, S., Batut, S., Fittschen, C.,
596 Thames, A. B., Brune, W. H., Ernest, C., Harder, H., Müller, J. B. A., Elste, T., Kubistin,
597 D., Andres, S., Bohn, B., Hohaus, T., Holland, F., Li, X., Rohrer, F., Kiendler-Scharr, A.,
598 Tillmann, R., Wegener, R., Yu, Z. J., Zou, Q., and Wahner, A.: Comparison of OH
599 reactivity measurements in the atmospheric simulation chamber SAPHIR, *Atmospheric
600 Measurement Techniques*, 10, 4023-4053, 2017.

601 Goldstein, A. H., and Galbally, I. E.: Known and unexplored organic constituents in the earth's
602 atmosphere, *Environmental Science & Technology*, 41, 1514-1521, 2007.

603 Gong, D. C., Wang, H., Zhang, S. Y., Wang, Y., Liu, S. C., Guo, H., Shao, M., He, C. R., Chen,
604 D. H., He, L. Y., Zhou, L., Morawska, L., Zhang, Y. H., and Wang, B. G.: Low-level
605 summertime isoprene observed at a forested mountaintop site in southern China:
606 implications for strong regional atmospheric oxidative capacity, *Atmospheric Chemistry
607 and Physics*, 18, 14417-14432, 10.5194/acp-18-14417-2018, 2018.

608 Graus, M., Müller, M., and Hansel, A.: High Resolution PTR-TOF: Quantification and Formula
609 Confirmation of VOC in Real Time, *J Am Soc Mass Spectr*, 21, 1037-1044, 2010.

610 Gueneron, M., Erickson, M. H., VanderSchelden, G. S., and Jobson, B. T.: PTR-MS
611 fragmentation patterns of gasoline hydrocarbons, *International Journal of Mass
612 Spectrometry*, 379, 97-109, 10.1016/j.ijms.2015.01.001, 2015.

613 Hansen, R. F., Griffith, S. M., Dusanter, S., Rickly, P. S., Stevens, P. S., Bertman, S. B., Carroll,
614 M. A., Erickson, M. H., Flynn, J. H., Grossberg, N., Jobson, B. T., Lefer, B. L., and

615 Wallace, H. W.: Measurements of total hydroxyl radical reactivity during CABINEX
616 2009-Part 1: field measurements, *Atmospheric Chemistry and Physics*, 14, 2923-2937,
617 10.5194/acp-14-2923-2014, 2014.

618 Hansen, R. F., Blocquet, M., Schoemaeker, C., Leonardis, T., Locoge, N., Fittschen, C.,
619 Hanoune, B., Stevens, P. S., Sinha, V., and Dusanter, S.: Intercomparison of the
620 comparative reactivity method (CRM) and pump-probe technique for measuring total OH
621 reactivity in an urban environment, *Atmospheric Measurement Techniques*, 8, 4243-
622 4264, 10.5194/amt-8-4243-2015, 2015.

623 Henry, S. B., Kammrath, A., and Keutsch, F. N.: Quantification of gas-phase glyoxal and
624 methylglyoxal via the Laser-Induced Phosphorescence of (methyl)GLyOxal
625 Spectrometry (LIPGLOS) Method, *Atmospheric Measurement Techniques*, 5, 181-192,
626 10.5194/amt-5-181-2012, 2012.

627 Herndon, S. C., Jayne, J. T., Zahniser, M. S., Worsnop, D. R., Knighton, B., Alwine, E., Lamb,
628 B. K., Zavala, M., Nelson, D. D., McManus, J. B., Shorter, J. H., Canagaratna, M. R.,
629 Onasch, T. B., and Kolb, C. E.: Characterization of urban pollutant emission fluxes and
630 ambient concentration distributions using a mobile laboratory with rapid response
631 instrumentation, *Faraday Discussions*, 130, 327-339, 10.1039/b500411j, 2005.

632 Hewitt, C. N., Lee, J. D., MacKenzie, A. R., Barkley, M. P., Carslaw, N., Carver, G. D.,
633 Chappell, N. A., Coe, H., Collier, C., Commane, R., Davies, F., Davison, B., Di Carlo, P.,
634 Di Marco, C. F., Dorsey, J. R., Edwards, P. M., Evans, M. J., Fowler, D., Furneaux, K.
635 L., Gallagher, M., Guenther, A., Heard, D. E., Helfter, C., Hopkins, J., Ingham, T., Irwin,
636 M., Jones, C., Karunaharan, A., Langford, B., Lewis, A. C., Lim, S. F., MacDonald, S.
637 M., Mahajan, A. S., Malpass, S., McFiggans, G., Mills, G., Misztal, P., Moller, S.,
638 Monks, P. S., Nemitz, E., Nicolas-Perea, V., Oetjen, H., Oram, D. E., Palmer, P. I.,
639 Phillips, G. J., Pike, R., Plane, J. M. C., Pugh, T., Pyle, J. A., Reeves, C. E., Robinson, N.
640 H., Stewart, D., Stone, D., Whalley, L. K., and Yin, X.: Overview: oxidant and particle
641 photochemical processes above a south-east Asian tropical rainforest (the OP3 project):
642 introduction, rationale, location characteristics and tools, *Atmospheric Chemistry and
643 Physics*, 10, 169-199, 10.5194/acp-10-169-2010, 2010.

644 Holzinger, R., Lee, A., Paw, K. T., and Goldstein, A. H.: Observations of oxidation products
645 above a forest imply biogenic emissions of very reactive compounds, *Atmospheric
646 Chemistry and Physics*, 5, 67-75, DOI 10.5194/acp-5-67-2005, 2005.

647 Holzinger, R.: PTRwid: A new widget tool for processing PTR-TOF-MS data, *Atmospheric
648 Measurement Techniques*, 8, 3903-3922, 10.5194/amt-8-3903-2015, 2015.

649 Jacob, D. J., Field, B. D., Jin, E. M., Bey, I., Li, Q. B., Logan, J. A., Yantosca, R. M., and Singh,
650 H. B.: Atmospheric budget of acetone, *Journal of Geophysical Research-Atmospheres*,
651 107, Artn 4100
652 10.1029/2001jd000694, 2002.

653 Jenkin, M. E., Saunders, S. M., and Pilling, M. J.: The tropospheric degradation of volatile
654 organic compounds: A protocol for mechanism development, *Atmospheric Environment*,
655 31, 81-104, Doi 10.1016/S1352-2310(96)00105-7, 1997.

656 Jeong, D., Seco, R., Gu, D., Lee, Y. R. O., Nault, B. A., Knote, C. J., Mcgee, T., Sullivan, J. T.,
657 Jimenez, J. L., Campuzano-Jost, P., Blake, D. R., Sanchez, D., Guenther, A. B., Tanner,
658 D., Huey, L. G., Long, R., Anderson, B. E., Hall, S. R., Ullmann, K., Shin, H. J.,
659 Herndon, S. C., Lee, Y. A. E., Kim, D., Ahn, O. O. Y., and Kim, S.: Integration of
660 airborne and ground observations of nitryl chloride in the Seoul metropolitan area and the

661 implications on regional oxidation capacity during KORUS-AQ 2016, *Atmospheric*
662 *Chemistry and Physics*, 19, 12779-12795, 10.5194/acp-19-12779-2019, 2019.

663 Jordan, A., Haidacher, S., Hanel, G., Hartungen, E., Mark, L., Seehauser, H., Schottkowsky, R.,
664 Sulzer, P., and Mark, T. D.: A high resolution and high sensitivity proton-transfer-
665 reaction time-of-flight mass spectrometer (PTR-TOF-MS), *International Journal of Mass*
666 *Spectrometry*, 286, 122-128, 2009a.

667 Jordan, A., Haidacher, S., Hanel, G., Hartungen, E., Märk, L., Seehauser, H., Schottkowsky, R.,
668 Sulzer, P., and Märk, T. D.: A high resolution and high sensitivity proton-transfer-
669 reaction time-of-flight mass spectrometer (PTR-TOF-MS), *Int J Mass Spectrom*, 286,
670 122-128, <http://dx.doi.org/10.1016/j.ijms.2009.07.005>, 2009b.

671 Kaiser, J., Skog, K. M., Baumann, K., Bertman, S. B., Brown, S. B., Brune, W. H., Crouse, J.
672 D., de Gouw, J. A., Edgerton, E. S., Feiner, P. A., Goldstein, A. H., Koss, A., Misztal, P.
673 K., Nguyen, T. B., Olson, K. F., St Clair, J. M., Teng, A. P., Toma, S., Wennberg, P. O.,
674 Wild, R. J., Zhang, L., and Keutsch, F. N.: Speciation of OH reactivity above the canopy
675 of an isoprene-dominated forest, *Atmospheric Chemistry and Physics*, 16, 9349-9359,
676 10.5194/acp-16-9349-2016, 2016.

677 Kim, S., Karl, T., Guenther, A., Tyndall, G., Orlando, J., Harley, P., Rasmussen, R., and Apel,
678 E.: Emissions and ambient distributions of Biogenic Volatile Organic Compounds
679 (BVOC) in a ponderosa pine ecosystem: interpretation of PTR-MS mass spectra,
680 *Atmospheric Chemistry and Physics*, 10, 1759-1771, 2010.

681 Kim, S., Guenther, A., Karl, T., and Greenberg, J.: Contributions of primary and secondary
682 biogenic VOC total OH reactivity during the CABINEX (Community Atmosphere-
683 Biosphere Interactions Experiments)-09 field campaign, *Atmospheric Chemistry and*
684 *Physics*, 11, 8613-8623, 10.5194/acp-11-8613-2011, 2011.

685 Kim, S., Wolfe, G. M., Mauldin, L., Cantrell, C., Guenther, A., Karl, T., Turnipseed, A.,
686 Greenberg, J., Hall, S. R., Ullmann, K., Apel, E., Hornbrook, R., Kajii, Y., Nakashima,
687 Y., Keutsch, F. N., DiGangi, J. P., Henry, S. B., Kaser, L., Schnitzhofer, R., Graus, M.,
688 Hansel, A., Zheng, W., and Flocke, F. F.: Evaluation of HOx sources and cycling using
689 measurement-constrained model calculations in a 2-methyl-3-butene-2-ol (MBO) and
690 monoterpene (MT) dominated ecosystem, *Atmospheric Chemistry and Physics*, 13, 2031-
691 2044, Doi 10.5194/Acp-13-2031-2013, 2013a.

692 Kim, S., Kim, S. Y., Lee, M., Shim, H., Wolfe, G. M., Guenther, A. B., He, A., Hong, Y., and
693 Han, J.: Impact of isoprene and HONO chemistry on ozone and OVOC formation in a
694 semirural South Korean forest, *Atmospheric Chemistry and Physics*, 15, 4357-4371, Doi
695 10.5194/Acp-15-4357-2015, 2015.

696 Kim, S., Sanchez, D., Wang, M. D., Seco, R., Jeong, D., Hughes, S., Barletta, B., Blake, D. R.,
697 Jung, J., Kim, D., Lee, G., Lee, M., Ahn, J., Lee, S.-D., Cho, G., Sung, M.-Y., Lee, Y.-
698 H., Kim, D. B., Kim, Y., Woo, J. H., Jo, D., Park, R., Park, J. H., Hong, Y.-D., and Hong,
699 J.-H.: OH Reactivity in Urban and Suburban regions in Seoul, South Korea-An East Asia
700 megacity in a rapid transition, *Faraday Discussions*, DOI:10.1039/C5FD00230C,
701 DOI:10.1039/C1035FD00230C, 2016.

702 Kim, S., Jeong, D., Sanchez, D., Wang, M., Seco, R., Blake, D., Meinardi, S., Barletta, B.,
703 Hughes, S., Jung, J., Kim, D., Lee, G., Lee, M., Ahn, J., Lee, S.-D., Cho, G., Sung, M.-
704 Y., Lee, Y.-H., and Park, R.: The Controlling Factors of Photochemical Ozone
705 Production in Seoul, South Korea, *Aerosol Air Qual Res*, 18, 2253-2261,
706 10.4209/aaqr.2017.11.0452, 2018.

707 Kim, S. Y., Jiang, X. Y., Lee, M., Turnipseed, A., Guenther, A., Kim, J. C., Lee, S. J., and Kim,
708 S.: Impact of biogenic volatile organic compounds on ozone production at the Taehwa
709 Research Forest near Seoul, South Korea, *Atmospheric Environment*, 70, 447-453, Doi
710 10.1016/J.Atmosenv.2012.11.005, 2013b.

711 Koss, A., Yuan, B., Warneke, C., Gilman, J. B., Lerner, B. M., Veres, P. R., Peischl, J.,
712 Eilerman, S., Wild, R., Brown, S. S., Thompson, C. R., Ryerson, T., Hanisco, T., Wolfe,
713 G. M., Clair, J. M. S., Thayer, M., Keutsch, F. N., Murphy, S., and de Gouw, J.:
714 Observations of VOC emissions and photochemical products over US oil- and gas-
715 producing regions using high-resolution H₃O⁺ CIMS (PTR-ToF-MS), *Atmos. Meas.*
716 *Tech.*, 10, 2941-2968, 10.5194/amt-10-2941-2017, 2017a.

717 Koss, A., Yuan, B., Warneke, C., Gilman, J. B., Lerner, B. M., Veres, P. R., Peischl, J.,
718 Eilerman, S., Wild, R., Brown, S. S., Thompson, C. R., Ryerson, T., Hanisco, T., Wolfe,
719 G. M., Clair, J. M. S., Thayer, M., Keutsch, F. N., Murphy, S., and de Gouw, J.:
720 Observations of VOC emissions and photochemical products over US oil- and gas-
721 producing regions using high-resolution H₃O⁺ CIMS (PTR-ToF-MS), *Atmospheric*
722 *Measurement Techniques*, 10, 2941-2968, 10.5194/amt-10-2941-2017, 2017b.

723 Kovacs, T. A., Brune, W. H., Harder, H., Martinez, M., Simpjas, J. B., Frost, G. J., Williams, E.,
724 Jobson, T., Stroud, C., Young, V., Fried, A., and Wert, B.: Direct measurements of urban
725 OH reactivity during Nashville SOS in summer 1999, *Journal of Environmental*
726 *Monitoring*, 5, 68-74, 10.1039/b204339d, 2003.

727 Kwok, E. S. C., and Atkinson, R.: Estimation of Hydroxyl Radical Reaction-Rate Constants for
728 Gas-Phase Organic-Compounds Using a Structure-Reactivity Relationship - an Update,
729 *Atmospheric Environment*, 29, 1685-1695, Doi 10.1016/1352-2310(95)00069-B, 1995.

730 Lee, A., Goldstein, A. H., Kroll, J. H., Ng, N. L., Varutbangkul, V., Flagan, R. C., and Seinfeld,
731 J. H.: Gas-phase products and secondary aerosol yields from the photooxidation of 16
732 different terpenes, *Journal of Geophysical Research-Atmospheres*, 111, Artn D17305
733 10.1029/2006jd007050, 2006.

734 Mao, J. Q., Ren, X. R., Chen, S. A., Brune, W. H., Chen, Z., Martinez, M., Harder, H., Lefer, B.,
735 Rappengluck, B., Flynn, J., and Leuchner, M.: Atmospheric oxidation capacity in the
736 summer of Houston 2006: Comparison with summer measurements in other metropolitan
737 studies, *Atmospheric Environment*, 44, 4107-4115, 10.1016/j.atmosenv.2009.01.013,
738 2010.

739 Muller, M., Graus, M., Wisthaler, A., Hansel, A., Metzger, A., Dommen, J., and Baltensperger,
740 U.: Analysis of high mass resolution PTR-TOF mass spectra from 1,3,5-trimethylbenzene
741 (TMB) environmental chamber experiments, *Atmospheric Chemistry and Physics*, 12,
742 829-843, 10.5194/acp-12-829-2012, 2012.

743 Nakashima, Y., Kato, S., Greenberg, J., Harley, P., Karl, T., Turnipseed, A., Apel, E., Guenther,
744 A., Smith, J., and Kajii, Y.: Total OH reactivity measurements in ambient air in a
745 southern Rocky mountain ponderosa pine forest during BEACHON-SRM08 summer
746 campaign, *Atmospheric Environment*, 85, 1-8, 2014.

747 Nolscher, A. C., Williams, J., Sinha, V., Custer, T., Song, W., Johnson, A. M., Axinte, R.,
748 Bozem, H., Fischer, H., Pouvesle, N., Phillips, G., Crowley, J. N., Rantala, P., Rinne, J.,
749 Kulmala, M., Gonzales, D., Valverde-Canossa, J., Vogel, A., Hoffmann, T., Ouwersloot,
750 H. G., de Arellano, J. V. G., and Lelieveld, J.: Summertime total OH reactivity
751 measurements from boreal forest during HUMPPA-COPEC 2010, *Atmospheric*
752 *Chemistry and Physics*, 12, 8257-8270, Doi 10.5194/Acp-12-8257-2012, 2012.

753 Nolscher, A. C., Yanez-Serrano, A. M., Wolff, S., de Araujo, A. C., Lavric, J. V., Kesselmeier,
754 J., and Williams, J.: Unexpected seasonality in quantity and composition of Amazon
755 rainforest air reactivity, *Nature Communications*, 7, ARTN 10383
756 10.1038/ncomms10383, 2016.

757 Ortega, J., Turnipseed, A., Guenther, A. B., Karl, T. G., Day, D. A., Gochis, D., Huffman, J. A.,
758 Prenni, A. J., Levin, E. J. T., Kreidenweis, S. M., DeMott, P. J., Tobo, Y., Patton, E. G.,
759 Hodzic, A., Cui, Y. Y., Harley, P. C., Hornbrook, R. S., Apel, E. C., Monson, R. K.,
760 Eller, A. S. D., Greenberg, J. P., Barth, M. C., Campuzano-Jost, P., Palm, B. B., Jimenez,
761 J. L., Aiken, A. C., Dubey, M. K., Geron, C., Offenberg, J., Ryan, M. G., Fornwalt, P. J.,
762 Pryor, S. C., Keutsch, F. N., DiGangi, J. P., Chan, A. W. H., Goldstein, A. H., Wolfe, G.
763 M., Kim, S., Kaser, L., Schnitzhofer, R., Hansel, A., Cantrell, C. A., Mauldin, R. L., and
764 Smith, J. N.: Overview of the Manitou Experimental Forest Observatory: site description
765 and selected science results from 2008 to 2013, *Atmospheric Chemistry and Physics*, 14,
766 6345-6367, 10.5194/acp-14-6345-2014, 2014.

767 Praplan, A. P., Tykka, T., Chen, D., Boy, M., Taipale, D., Vakkari, V., Zhou, P. T., Petaja, T.,
768 and Hellen, H.: Long-term total OH reactivity measurements in a boreal forest,
769 *Atmospheric Chemistry and Physics*, 19, 14431-14453, 10.5194/acp-19-14431-2019,
770 2019.

771 Ramasamy, S., Nagai, Y., Takeuchi, N., Yamasaki, S., Shojia, K., Ida, A., Jones, C., Tsurumaru,
772 H., Suzuki, Y., Yoshino, A., Shimada, K., Nakashima, Y., Kato, S., Hatakeyama, S.,
773 Matsuda, K., and Kajii, Y.: Comprehensive measurements of atmospheric OH reactivity
774 and trace species within a suburban forest near Tokyo during AQUAS-TAMA campaign,
775 *Atmospheric Environment*, 184, 166-176, 10.1016/j.atmosenv.2018.04.035, 2018.

776 Ren, X. R., Harder, H., Martinez, M., Leshner, R. L., Olinger, A., Shirley, T., Adams, J., Simpas, J.
777 B., and Brune, W. H.: HO_x concentrations and OH reactivity observations in New York
778 City during PMTACS-NY2001, *Atmospheric Environment*, 37, 3627-3637,
779 10.1016/S1352-2310(03)00460-6, 2003.

780 Ren, X. R., Brune, W. H., Olinger, A., Metcalf, A. R., Simpas, J. B., Shirley, T., Schwab, J. J.,
781 Bai, C. H., Roychowdhury, U., Li, Y. Q., Cai, C. X., Demerjian, K. L., He, Y., Zhou, X.
782 L., Gao, H. L., and Hou, J.: OH, HO₂, and OH reactivity during the PMTACS-NY
783 Whiteface Mountain 2002 campaign: Observations and model comparison, *Journal of*
784 *Geophysical Research-Atmospheres*, 111, Artn D10s03
785 10.1029/2005jd006126, 2006.

786 Rinne, J., Ruuskanen, T. M., Reissell, A., Taipale, R., Hakola, H., and Kulmala, M.: On-line
787 PTR-MS measurements of atmospheric concentrations of volatile organic compounds in
788 a European boreal forest ecosystem, *Boreal Environ Res*, 10, 425-436, 2005.

789 Ruuskanen, T. M., Mueller, M., Schnitzhofer, R., Karl, T., Graus, M., Bamberger, I., Hortnagl,
790 L., Brilli, F., Wohlfahrt, G., and Hansel, A.: Eddy covariance VOC emission and
791 deposition fluxes above grassland using PTR-TOF, *Atmospheric Chemistry and Physics*,
792 11, 611-625, 2011.

793 Sanchez, D., Jeong, D., Seco, R., Wrangham, I., Park, J.-H., Brune, W. H., Koss, A., Gilman, J.,
794 de Gouw, J., Misztal, P., Goldstein, A., Baumann, K., Wennberg, P. O., Keutsch, F. N.,
795 Guenther, A., and Kim, S.: Intercomparison of OH and OH reactivity measurements in a
796 high isoprene and low NO environment during the Southern Oxidant and Aerosol Study
797 (SOAS), *Atmospheric Environment*, 174, 227-236, 10.1016/j.atmosenv.2017.10.056,
798 2018.

799 Sanchez, D.: Towards the closure of OH reactivity and volatile organic compound budget in the
800 troposphere using in situ observations, Ph. D., Department of Earth System Science,
801 University of California, Irvine, 2019.

802 Saunders, S. M., Jenkin, M. E., Derwent, R. G., and Pilling, M. J.: Protocol for the development
803 of the Master Chemical Mechanism, MCM v3 (Part A): tropospheric degradation of non-
804 aromatic volatile organic compounds, *Atmospheric Chemistry and Physics*, 3, 161-180,
805 2003.

806 Seco, R., Penuelas, J., and Filella, I.: Short-chain oxygenated VOCs: Emission and uptake by
807 plants and atmospheric sources, sinks, and concentrations, *Atmospheric Environment*, 41,
808 2477-2499, 10.1016/j.atmosenv.2006.11.029, 2007.

809 Shirley, T. R., Brune, W. H., Ren, X., Mao, J., Leshner, R., Cardenas, B., Volkamer, R., Molina,
810 L. T., Molina, M. J., Lamb, B., Velasco, E., Jobson, T., and Alexander, M.: Atmospheric
811 oxidation in the Mexico City Metropolitan Area (MCMA) during April 2003,
812 *Atmospheric Chemistry and Physics*, 6, 2753-2765, DOI 10.5194/acp-6-2753-2006,
813 2006.

814 Sinha, V., Williams, J., Crowley, J. N., and Lelieveld, J.: The comparative reactivity method - a
815 new tool to measure total OH reactivity in ambient air, *Atmospheric Chemistry and
816 Physics*, 8, 2213-2227, 2008a.

817 Sinha, V., Williams, J., Crowley, J. N., and Lelieveld, J.: The Comparative Reactivity Method
818 ‐ a new tool to measure total OH Reactivity in ambient air, *Atmos. Chem. Phys.*,
819 8, 2213-2227, 10.5194/acp-8-2213-2008, 2008b.

820 Sinha, V., Williams, J., Lelieveld, J., Ruuskanen, T. M., Kajos, M. K., Patokoski, J., Hellen, H.,
821 Hakola, H., Mogensen, D., Boy, M., Rinne, J., and Kulmala, M.: OH Reactivity
822 Measurements within a Boreal Forest: Evidence for Unknown Reactive Emissions,
823 *Environmental Science & Technology*, 44, 6614-6620, Doi 10.1021/Es101780b, 2010.

824 Sinha, V., Williams, J., Diesch, J. M., Drewnick, F., Martinez, M., Harder, H., Regelin, E.,
825 Kubistin, D., Bozem, H., Hosaynali-Beygi, Z., Fischer, H., Andres-Hernandez, M. D.,
826 Kartal, D., Adame, J. A., and Lelieveld, J.: Constraints on instantaneous ozone
827 production rates and regimes during DOMINO derived using in-situ OH reactivity
828 measurements, *Atmospheric Chemistry and Physics*, 12, 7269-7283, Doi 10.5194/Acp-
829 12-7269-2012, 2012.

830 Sullivan, J. T., McGee, T. J., Stauffer, R. M., Thompson, A. M., Weinheimer, A., Knute, C.,
831 Janz, S., Wisthaler, A., Long, R., Szykman, J., Park, J., Lee, Y., Kim, S., Jeong, D.,
832 Sanchez, D., Twigg, L., Sunnicht, G., Knepp, T., and Schroeder, J. R.: Taehwa Research
833 Forest: a receptor site for severe domestic pollution events in Korea during 2016,
834 *Atmospheric Chemistry and Physics*, 19, 5051-5067, 10.5194/acp-19-5051-2019, 2019.

835 Whalley, L. K., Stone, D., Bandy, B., Dunmore, R., Hamilton, J. F., Hopkins, J., Lee, J. D.,
836 Lewis, A. C., and Heard, D. E.: Atmospheric OH reactivity in central London:
837 observations, model predictions and estimates of in situ ozone production, *Atmospheric
838 Chemistry and Physics*, 16, 2109-2122, 10.5194/acp-16-2109-2016, 2016.

839 Williams, J., Poschl, U., Crutzen, P. J., Hansel, A., Holzinger, R., Warneke, C., Lindinger, W.,
840 and Lelieveld, J.: An atmospheric chemistry interpretation of mass scans obtained from a
841 proton transfer mass spectrometer flown over the tropical rainforest of Surinam, *Journal
842 of Atmospheric Chemistry*, 38, 133-166, Doi 10.1023/A:1006322701523, 2001.

843 Yang, Y. D., Shao, M., Wang, X. M., Nolscher, A. C., Kessel, S., Guenther, A., and Williams, J.:
844 Towards a quantitative understanding of total OH reactivity: A review, *Atmospheric*
845 *Environment*, 134, 147-161, 10.1016/j.atmosenv.2016.03.010, 2016.

846 Yang, Y. D., Shao, M., Kessel, S., Li, Y., Lu, K. D., Lu, S. H., Williams, J., Zhang, Y. H., Zeng,
847 L. M., Noelscher, A. C., Wu, Y. S., Wang, X. M., and Zheng, J. Y.: How the OH
848 reactivity affects the ozone production efficiency: case studies in Beijing and Heshan,
849 China, *Atmospheric Chemistry and Physics*, 17, 7127-7142, 10.5194/acp-17-7127-2017,
850 2017.

851 Yuan, B., Warneke, C., Shao, M., and de Gouw, J. A.: Interpretation of volatile organic
852 compound measurements by proton-transfer-reaction mass spectrometry over the
853 deepwater horizon oil spill, *International Journal of Mass Spectrometry*, 358, 43-48,
854 10.1016/j.ijms.2013.11.006, 2014.

855 Zannoni, N., Gros, V., Esteve, R. S., Kalogridis, C., Michoud, V., Dusanter, S., Sauvage, S.,
856 Locoge, N., Colomb, A., and Bonsang, B.: Summertime OH reactivity from a receptor
857 coastal site in the Mediterranean Basin, *Atmospheric Chemistry and Physics*, 17, 12645-
858 12658, 2017.

859 Zhao, J., Zhang, R. Y., Fortner, E. C., and North, S. W.: Quantification of hydroxycarbonyls
860 from OH-isoprene reactions, *J Am Chem Soc*, 126, 2686-2687, 10.1021/ja0386391,
861 2004.

863

864

865

866 **Tables and Figures**

867

868 Table 1. Description of instrument and measured parameters.

Instrument	Parameters	Measurement Uncertainty (1σ) and lower level of detection limit
Chemical Ionization Spectroscopy - Comparative Reactivity Method (CIMS-CRM)	OH reactivity	16.7% (5 sec ⁻¹)
Thermo Scientific 42i	NO	20% (100 ppt)
Cavity Ring Down Spectroscopy	NO ₂	20% (50 ppt)
Thermo Scientific 49i	O ₃	4% (1 ppb)
Lufft 501 C	Temperature	±0.3 °C (NA)
Thermo Scientific 48i TLE	CO	10% (50 ppb)

Thermo Scientific 43i TLE	SO ₂	10% (100 ppt)
Mini Tunable Infrared Laser Direct Absorption Spectroscopy (mini-TILDAS) Formaldehyde Monitor(Herndon et al., 2005) (Aerodyne Research, Inc)	HCHO, CH ₄ , CH ₃ OH	5% (few tens ppt)
Proton Transfer Reaction Time of Flight Mass Spectrometer (PTR-TOF-MS 8000, IONICON Analytik, GmbH)	Acetaldehyde, Ethanol, Acetone, Isoprene, MVK + MACR, Methyl ethyl ketone, Benzene, Monoterpenes, Toluene, Furfural, Benzaldehyde, Xylenes, Trimethylbenzenes, Sesquiterpenes	Isoprene 9.8% Benzene 6.9% Toluene 6.5% Monoterpenes 9.2% Xylenes 4.0% Other 16.5% (tens ppt)

869

870

871

872

873

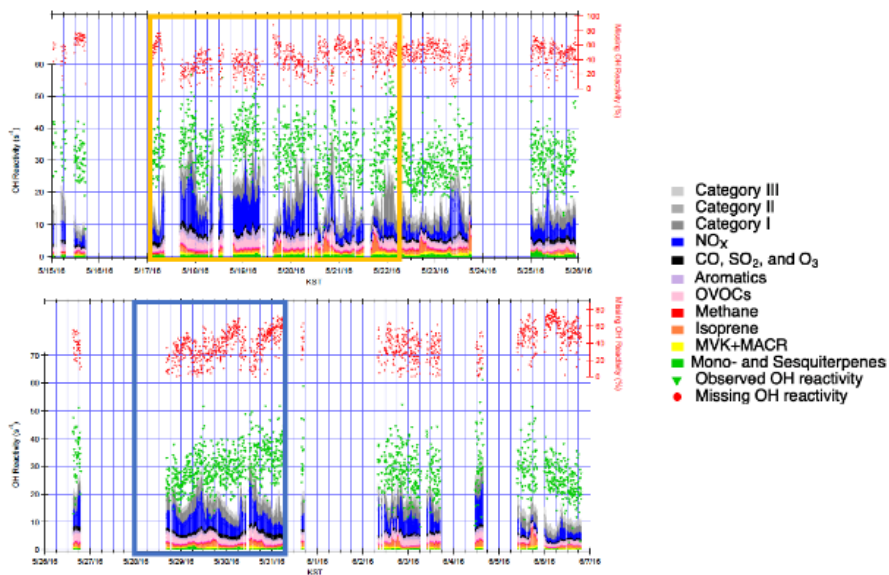
874

875 Figure 1. Observed and calculated OH reactivity during KORUS-AQ 2016. The measured and

876 calculated OH reactivity are on the left axis while the missing OH reactivity is on the right axis.

877 The yellow box represents the stagnation period and the blue box represents the transport period.

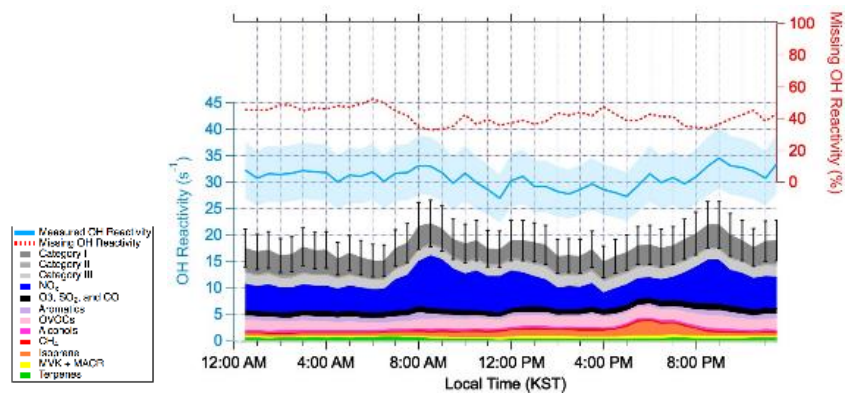
878



879

880

881 Figure 2. The diurnal average of OH reactivity from 15 May 2016 – 7 June 2016. The measured
882 and calculated OH reactivity are on the left axis. The blue shading represents uncertainty in the
883 measured OH reactivity. The black bars represent the propagated uncertainty of calculated OH
884 reactivity. The missing OH Reactivity in the percentage scale can be read using the right axis.
885



886

887

888

889

890

891

892

893

894

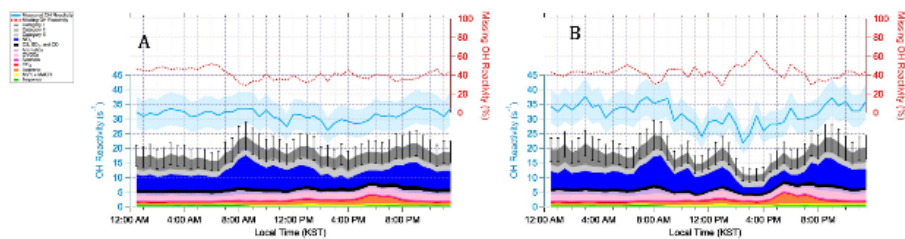
895

896

897

898 Figure 3. Diurnal averages of OH reactivity during the stagnation period (A) from May 17th –
899 May 22nd in 2016 and the transport period (B) from 28 May – 1 June 2016. The measured and
900 calculated OH reactivity are on the left. The blue shading represents an uncertainty of 16.7% at
901 1σ . The black bars represent the propagated uncertainty of 20.1% at 1σ from calculated missing
902 OH reactivity. The percent missing OH reactivity is on the right axis.

903



904

905

906

907

908

909

910

911

912

913

914

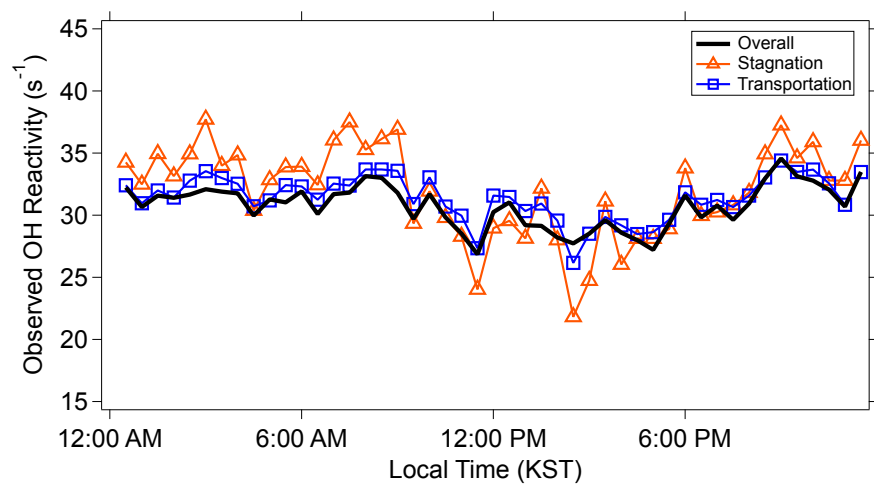
915

916

917 Figure 4. The observed OH reactivity during the overall campaign, stagnation period, and

918 transport period.

919



920

921

922

923

924

925

926

927

928

929

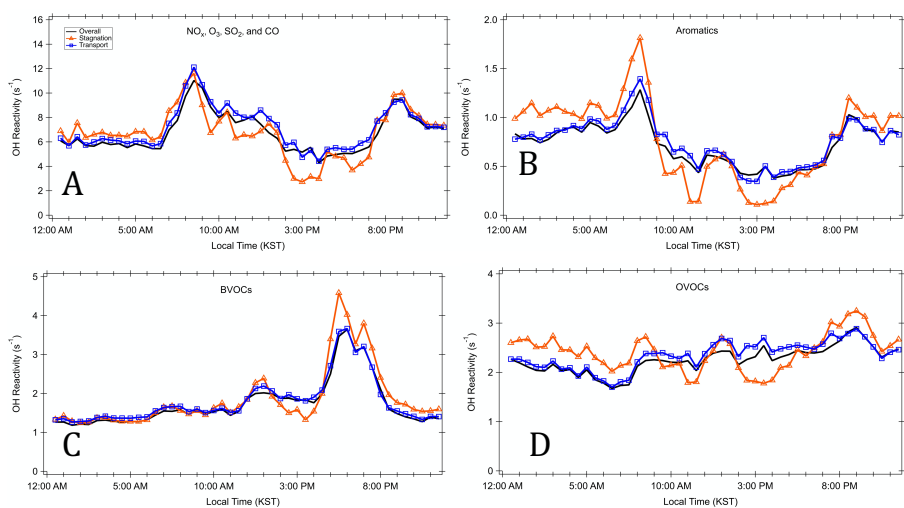
930

931 Figure 5. Diurnal profiles for different classes of trace gases during the different periods. A)

932 criteria pollutants NO_x , O_3 , SO_2 , and CO B) Aromatics, C) BVOCs, and D) OVOCs

933

934



935

936

937

938

939

940

941

942

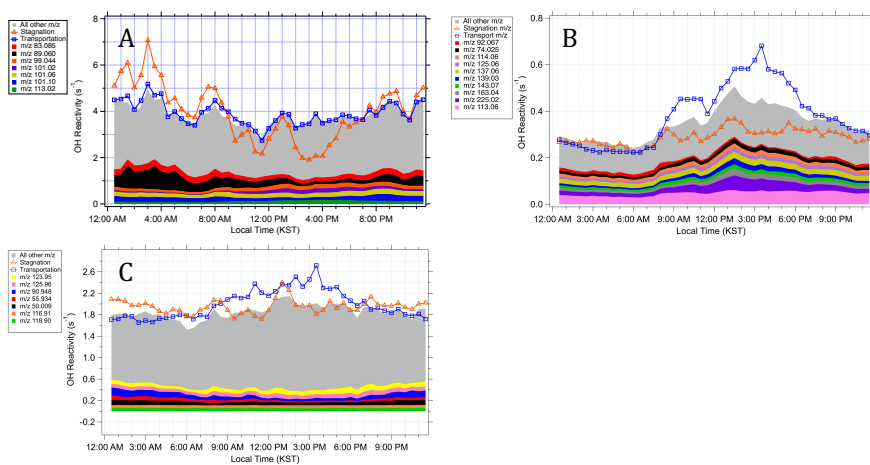
943

944

945 Figure 6. Diurnal averages of the OH reactivity from the compounds in A) Category I, B)

946 Category II and C) Category III

947



948

949

950

951

952

953

954

955

956

957

958

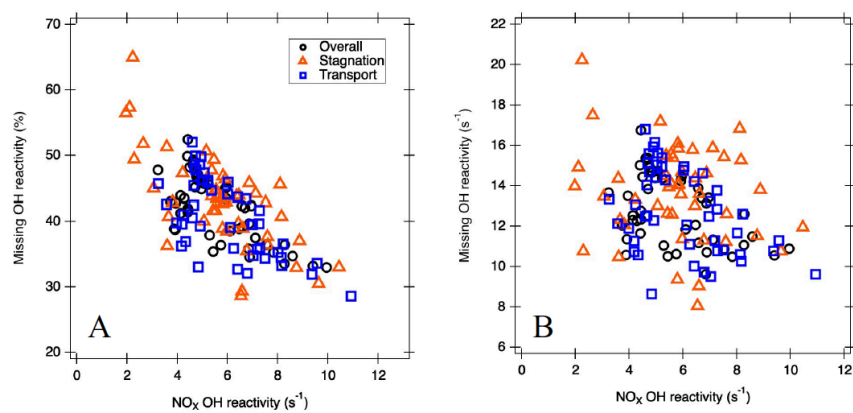
959

960

961 Figure 7. The correlation between A) NO_x OH reactivity and absolute missing OH reactivity and
962 B) percent missing OH reactivity

963

964



965